separations

MDPI

Article

A Study on the Removal Characteristics and Mechanism of Phosphorus from Simulated Wastewater Using a Novel Modified Red-Mud-Based Adsorption Material

Wenbao Liu [1,2], Qin Zhang [1,*], Yanbai Shen [2,*], Weichao Li [2], Sikai Zhao [2], Qiang Zhao [2] and Yiqun Zhang [2]

[1] Guizhou Academy of Science, Guiyang 550001, China; liuwenbao@mail.neu.edu.cn
[2] School of Resources & Civil Engineering, Northeastern University, Shenyang 110819, China; lwc19950517@163.com (W.L.); zhaosikai@mail.neu.edu.cn (S.Z.); zhaoqiang@mail.neu.edu.cn (Q.Z.); 20191771@stu.neu.edu.cn (Y.Z.)
* Correspondence: zq6736@163.com (Q.Z.); shenyanbai@mail.neu.edu.cn (Y.S.)

Abstract: In this work, a common third-generation environmentally friendly quaternary ammonium salt disinfectant, dimethyl dioctadecyl ammonium chloride (DDAC), was used as the modifier to achieve one-step rapid preparation of the modified red-mud-based adsorption material under the condition of microwave assistance, and applied it to the adsorption phosphorus in solutions. After the process of this modification, the structure of the red mud (RM) was not changed, and the DDAC modification could provide more adsorption active sites. The adsorption experiments indicated that the novel modified red mud (NMRM) exhibited a good adsorption performance for phosphorus. The adsorption capability of NMRM for phosphorus was significantly enhanced, and was about eight times higher than that of the initial RM. The kinetics model of the pseudo-second-order, which implied that phosphorus was chemically adsorbed on the surface of the NMRM, could accurately represent the adsorption procedure of NMRM. The adsorption equilibrium of NMRM could be better depicted using the isotherm model of Freundlich. It was speculated that the ion exchange might be responsible for the adsorption mechanism of NMRM for phosphorus. Thus, the NMRM is a potential material for the treatment of phosphorus-containing wastewater due to its outstanding adsorption capability.

Keywords: red mud; modification; ion exchange; phosphorus; adsorption

check for updates

Citation: Liu, W.; Zhang, Q.; Shen, Y.; Li, W.; Zhao, S.; Zhao, Q.; Zhang, Y. A Study on the Removal Characteristics and Mechanism of Phosphorus from Simulated Wastewater Using a Novel Modified Red-Mud-Based Adsorption Material. *Separations* **2023**, *10*, 562. https://doi.org/10.3390/separations10110562

Academic Editor: Sascha Nowak

Received: 18 October 2023
Revised: 7 November 2023
Accepted: 8 November 2023
Published: 10 November 2023

Copyright: © 2023 by the authors. Licensee MDPI, Basel, Switzerland. This article is an open access article distributed under the terms and conditions of the Creative Commons Attribution (CC BY) license (https://creativecommons.org/licenses/by/4.0/).

1. Introduction

Red mud (RM) is a red-polluting solid industrial waste generated during the production of aluminum oxide [1]. For every ton of aluminum oxide produced, 1–2 tonnes of RM would be produced [2]. However, with the high-quality bauxite deposits used up, the bauxite grade continues to drop, leading to an increase in RM production during the production of aluminum oxide [3]. RM, as a bulk solid waste in aluminum oxide production, has a comprehensive utilization rate of less than 6%, and most RM is piled up [4]. RM is basically stored in the open air, occupying a large amount of land [5]. Due to the high alkalinity of red mud, its stockpiling over a long time not only uses considerable land resources, but also results in air pollution and land alkalization, thereby contaminating the groundwater, and it also results in a lot of maintenance costs [1,6–9]. In addition, RM could erode dams because of its high alkalinity, which might pose serious safety issues [10].

The environmental pollution caused by the long-term storage of RM limits the sustainable growth of the aluminum sector. Therefore, to reduce the environmental pollution, global scholars have carried out various reuse studies according to the characteristics and composition of RM [11,12]. For the past several decades, the research on RM utilization has mainly focused on the valuable metal's recovery [13,14], the production of building materials [15,16], and reaction catalysts [17–19]. Recently, the physicochemical properties

of RM, for example its high dispersion and high specific surface area, have been widely considered by researchers. These features make it a potential adsorption material [7,20–23].

In recent years, eutrophication has become the most serious water pollution problem in many natural water bodies [24–26]. The primary cause of this issue is the massive discharge of phosphorus-containing wastewater from phosphorus chemical enterprises [27–29]. Eutrophication will directly change the physical and chemical characteristics of rivers and lakes, affect the living environment of aquatic organisms, and finally destroy the stability of aquatic ecosystems [30,31]. Therefore, strict phosphorus removal before wastewater discharge is an important way to prevent water eutrophication. The existing phosphorus removal methods mainly include biological methods [32,33] and chemical methods [25,34,35]. The biological process is mainly suitable for treating low-concentration and organic phosphorus-containing wastewater, but the control of phosphorus removal conditions is strict and the cost is high [36]. Chemical methods mainly include coagulation sedimentation, ion exchange, and reverse osmosis, which are normally suitable for the removal of inorganic and high-concentration phosphorus-containing wastewater, but these technologies are faced with complex operation and easy to produce secondary pollution and other issues [37–39]. The adsorption method has a low operating cost, high phosphorus removal efficiency, and does not easily produce secondary pollution, so it has strong applicability in actual industrial sewage treatment [40–42]. The development of highly effective adsorbents is a crucial goal for industrialization and environmental protection, since the absorbent is key to the adsorption process [43].

The physicochemical properties of RM make it display tremendous potential in the preparation of adsorbents. It will be environmentally advantageous with double benefits in cases where such a large variety of solid waste from industry could be utilized to remove phosphorus from wastewater with high efficiency, while, owing to the original RM's poor adsorption ability, it must be modified to enhance its adsorption ability [44]. Acidification, thermal treatment, organic modification, neutralization, composite material synthesis, and so on, are the common modification methods [45]. According to reports, these modifications enhanced the phosphorus adsorption effectiveness of the conventional adsorption material. In this paper, a common third-generation environmentally friendly quaternary ammonium salt disinfectant, dimethyl dioctadecyl ammonium chloride (DDAC), was first introduced in modifying RM to develop the novel high-efficiency adsorption material for phosphorus, combined with microwave-assisted conditions. The high efficiency of modified red mud has been confirmed by phosphorus adsorption experimental results. The adsorption kinetics, isotherms, and thermodynamics were also explored, and the adsorption mechanism of the modified red mud (NMRM) for phosphorous, based on the analysis results of scanning electron microscopy (SEM), energy dispersive spectrometer (EDS), Fourier transform infrared spectroscopy (FTIR), and zeta potential. This method makes full use of the resource contents of red mud, and greatly improves adsorption performance of red mud. The modification method is simple and easy to scale up. Therefore, it is demonstrated that the NMRM had good prospects for the cleanup of phosphorus-containing wastewater.

2. Experiment

2.1. Minerals and Reagents

The RM used in this study was obtained from a certain aluminum factory in Guizhou, China. The chemical composition of RM used for this study was examined via X-ray fluorescence spectroscopy (ARLAdvant X IntellipowerTM3600, ThermoFisher, Carlsbad, CA, USA). The analysis findings are displayed in Table 1. Trisodium phosphate anhydrous (Na_3PO_4), dimethyl dioctadecyl ammonium chloride (DDAC), ascorbic acid, ammonium molybdate, and potassium antimony tartrate were purchased from Macklin (Shanghai, China). Meanwhile, the sulfuric acid (H_2SO_4) used in the study was bought from Sinopharm Chemical Reagent Co., Ltd. (Shanghai, China). For all aqueous solutions in the study, deionized water was used.

Table 1. Chemical composition of RM (wt%).

Components	Al_2O_3	CaO	SiO_2	Fe_2O_3	TiO_2	K_2O	MgO	SO_3	Na_2O	ZrO_2	other
Content	25.95	25.51	19.59	14.62	7.36	2.61	2.08	0.74	0.73	0.26	0.57

2.2. Mechanism Analysis Methods

The micro-morphology, the distribution of surface elements, and their difference in terms of the initial RM before and after modification and adsorption were studied by scanning electron microscopy (SEM, FEI-QUANTA FEG250, Orlando, FL, USA) equipped with an energy dispersive spectrometry (EDS, JOEL-JSM-5910LV, Tokyo, Japan). Fourier transform infrared spectroscopy, which is Nicolet iS50 produced by Thermo, was utilized to investigate the infrared spectra of the initial RM before and after modification and adsorption and analyze their differences. The zeta potentials of the initial RM before and after modification and adsorption were measured using a zeta potential analyzer (Nano-ZS90, Malvern Panalytical, Malvern, UK). The crystal phase compositions and differences of RM and NMRM were investigated via an X-ray diffraction analyzer, which is D8 Advance produced by Bruker, Germany. The RM's and NMRM's specific surface area was measured and analyzed by Brunauer Emmett Tells (BET, ASAP 2020 Plus HD88, Micromeritics, Atlanta, GA, USA).

2.3. Analysis of P Concentration

The concentration of phosphorus was analyzed by spectrophotometry [46]. Taking a 1 mL solution to be tested in a 5 mL volumetric flask, add 0.1 mL of ascorbic acid solution to it, then add 3.7 mL of deionized water, mix for 30 s, then add 0.2 mL of molybdate solution, and stand for 15 min. After determining the sample's absorbance with an ultraviolet spectrophotometer (UV-8000, METASH, Shanghai, China) at its typical wavelength of 700 nm, the phosphorus (P) concentration of the solution was calculated employing the standard curve of concentration and absorbance for phosphorus (Figure 1).

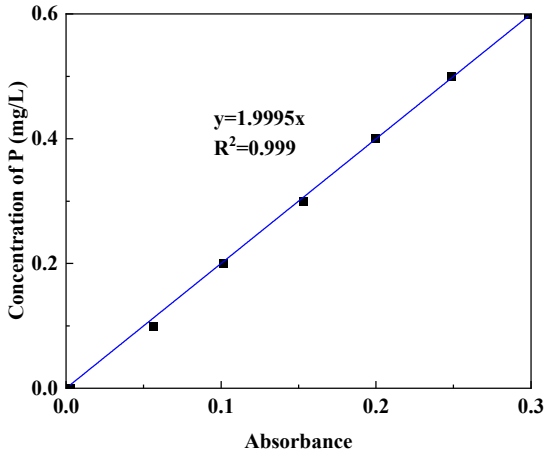


Figure 1. Standard curve for P's concentration–absorbance relationship.

2.4. Preparation of the NMRM

A certain amount of the initial RM tailings after magnetic separation was infused into the 20 mmol/L DDAC solution to perform the novel high-efficiency adsorption material for phosphorus NMRM. The solid-to-liquid ratio of samples in the preparation of the NMRM was 1:50. Then, the suspension that resulted was spread out using ultrasound for 5 min. Next, the above suspension was heated with a microwave oven for 10 min (power = 400 W). Finally, after being extracted from the suspension by high-speed centrifugation (6000 r/min), the samples of the NMRM were dried for 12 h at 90 °C. Figure 2 displays the preparation process of the NMRM.

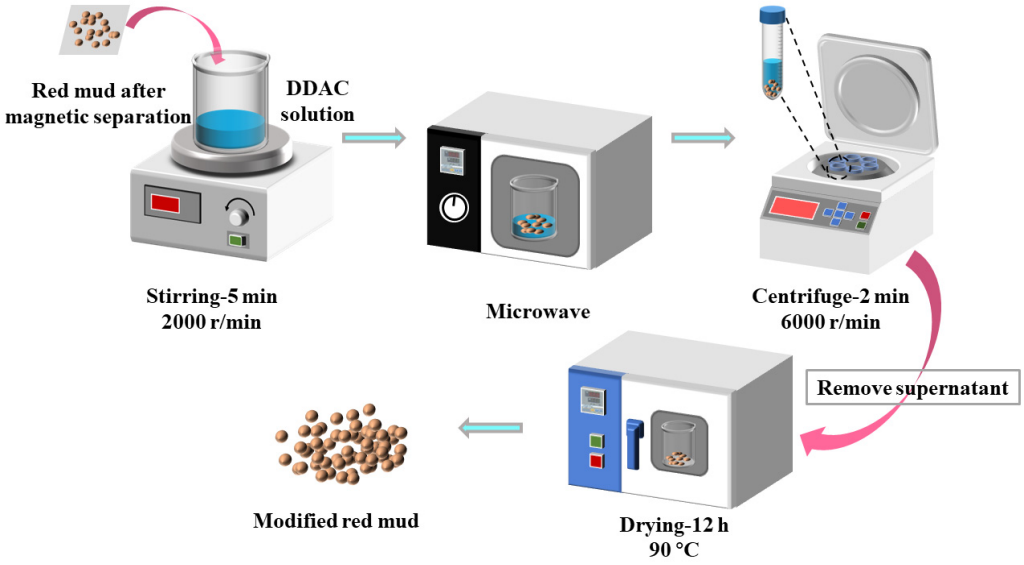


Figure 2. The preparation process of the NMRM.

2.5. Adsorption Experiments

The phosphorus solution (10 mL), with a concentration of 5–50 mg/L, was put into a tube of sealable plastic containing NMRM (0.5–6 mg/L). After adsorption for a certain time in a thermostatic shaker, the concentration of P in solutions was quantitatively determined using spectrophotometry. The adsorption quantity (q, mg/g) was calculated by Formula (1), and the adsorption efficiency (η, %) was computed by Formula (2).

$$q\ (\mathrm{mg/g}) = \frac{V(C_0 - C_1)}{m} \quad (1)$$

$$\eta\ (\%) = \frac{C_0 - C_1}{C_0} \times 100 \quad (2)$$

where V means the solution volume (mL), m means the adsorbent mass (g), and C_0 and C_1 represent P concentration (mg/L) in the solution before and after adsorption, respectively.

3. Results and Discussion

3.1. Characterization of the NMRM

To understand the morphology and elemental composition of the initial RM before and after modification, SEM and mapping EDS were performed. The results are displayed in Figures 3 and 4. The diameter of the initial RM particles before modification was smaller, and distributed evenly and loosely. The diameter of the initial RM particles modified by DDAC was larger. From Figure 4, it is obvious that the main elements of the initial RM were O, Si, P, and C. After modification, the content of C in NMRM obviously increased, and a new element N appeared, which indicated that DDAC was successfully loaded on the RM.

The static N_2-adsorption capacity technique was used to calculate the BET surface area for both samples (RM and NMRM). The BET analyses findings of RM and NMRM are presented in Table 2. It can be seen from Table 2 that the initial RM contained small particles, which became larger following the DDAC modification. After the modification, the RM's BET surface area lowered significantly, from 11.60 m^2/g to 0.52 m^2/g. Meanwhile, it was visible that the RM's total pore volume also lowered, and the values decreased from 0.057 cm^3/g to 0.004 cm^3/g, while after the modification, the average particle size of the RM rose from 19.73 nm to 31.32 nm. These suggest that the particle size of RM modified by DDAC increased, its specific surface area reduced, and the adsorption behavior could mainly depend on the adsorption sites of the NMRM-based adsorption material.

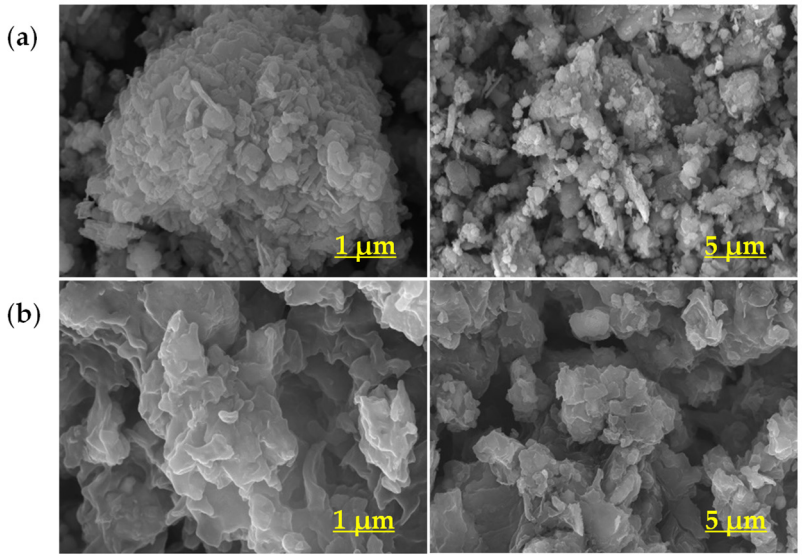


Figure 3. SEM images of the initial RM before (**a**) and after (**b**) modification.

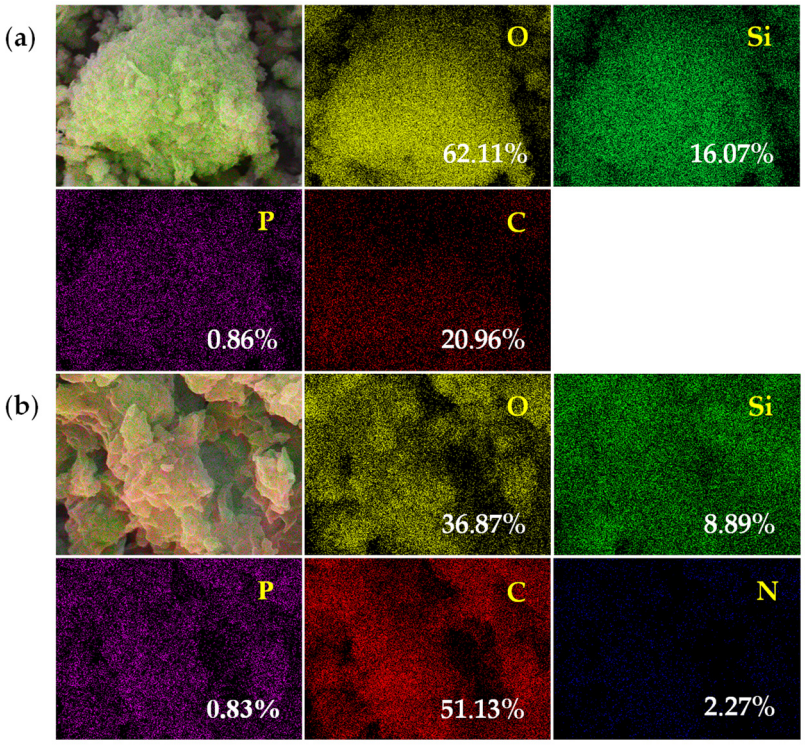


Figure 4. EDS mapping of the initial RM before (**a**) and after (**b**) modification.

Table 2. BET analyses of the initial RM before and after modification.

Samples	S_{BET} (m^2/g)	V_{Total} (cm^3/g)	D_{Aver} (nm)
Before modification	11.60	0.057	19.73
After modification	0.52	0.004	31.32

The FT-IR spectra of the initial RM before and after modification are displayed in Figure 5. The peaks that occurred at about 561 cm^{-1}, 620 cm^{-1}, and 679 cm^{-1} in the RM spectrum were linked to the stretching or bending vibrations of the Si-O tetrahedron or the Al-O tetrahedron functional group [47]. There was a peak at 1003 cm^{-1} in the FT-IR spectra of RM before and after modification, respectively, which corresponded to the Al-

O tetrahedron shift. After modification, a new absorption peak of 2916 cm^{-1} appeared in the RM spectrum, which is related to alkanes. Additionally, the absorption peaks of C_4N^+ at 1474 cm^{-1} also appeared on RM [48]. These features indicate that the DDAC was successfully loaded onto the RM, and the modification did not change the structure of the RM.

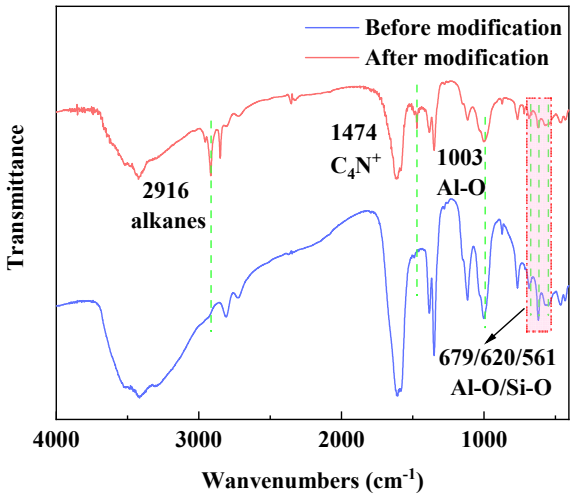


Figure 5. FT-IR spectra of RM before and after modification.

To investigate the influence of RM surface charge properties on adsorption, the zeta potentials of RM before and after modification were evaluated, which are displayed in Figure 6. It can be seen that the zeta potential of the NMRM was negative at pH > 11.2; however, that of the initial RM was negative at pH > 8.1. It also indicates that the increase of the initial RM's isoelectric point could be due to the adsorption of the bound N^+ ions on the NMRM surface [49]. Thus, the phosphorus ions with negative charges were easier to absorb on NMRM with more positive charges. The above findings were conformed to the results of FT-IR, which show that DDAC was successfully loaded onto the RM. The XRD analysis was used to compare the crystal phase composition difference of the RM and the NMRM, which is displayed in Figure 7. It is visible that the crystal phase composition of the RM had not changed before and after modification. The above analysis results show that the DDAC modification did not change the structure of RM, but could change the surface charge properties and might provide more active adsorption sites.

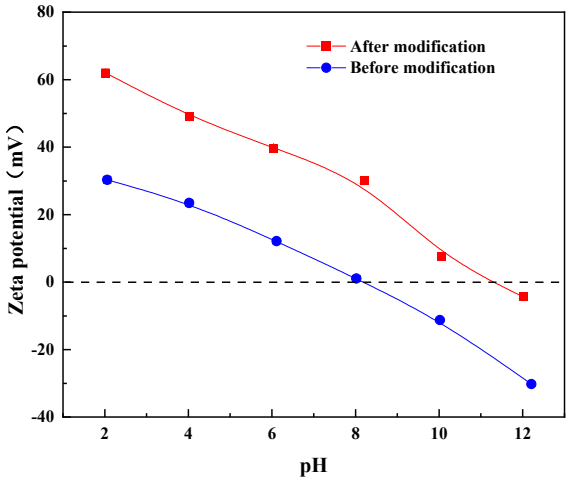


Figure 6. The relationship between the zeta potentials of RM or NMRM and pH value.

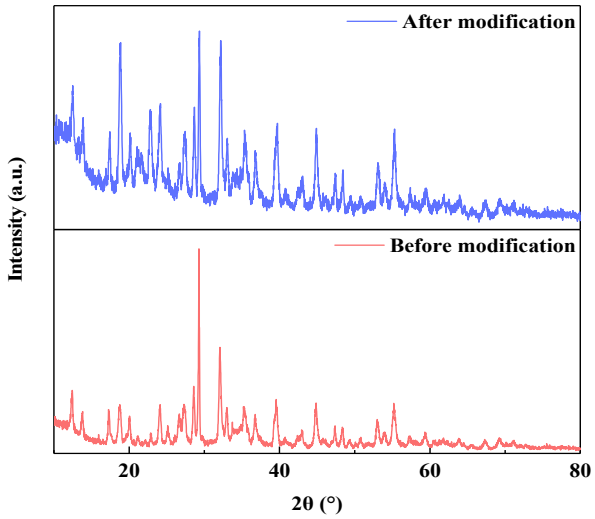


Figure 7. XRD patterns of RM and NMRM.

3.2. Adsorption Performance of the NMRM for P

To study the influence of the NMRM dosage for P adsorption, different NMRM dosages were introduced into the solution to obtain the optimal condition of NMRM for removing P from the solution. The findings are displayed in Figure 8. It is evident that, with an increase in the NMRM dosage, the adsorption of phosphorus first increased and then tended to be steady, while the adsorption capacity of phosphorus slowly decreased. This is mainly because when the adsorbent dosage is low, the adsorbent will soon reach adsorption saturation, and then increasing the adsorbent dosage will reduce the unit adsorption capacity of the adsorbent [50]. When the NMRM dosage was 4 mg/L, the phosphorus adsorption efficiency reached the maximum, the phosphorus adsorption efficiency of NMRM was 90.56%, and the adsorption capacity was 2.29 mg/g. It is also visible that, at an NMRM dosage of 2 mg/L, the adsorption efficiency was 87.8%, and the adsorption capacity was 4.41 mg/g. Although the adsorption efficiency at this time was slightly lower than that at 4 mg/L, the adsorption capacity was higher. Therefore, the NMRM dosage was 2 mg/L in the subsequent adsorption experiment.

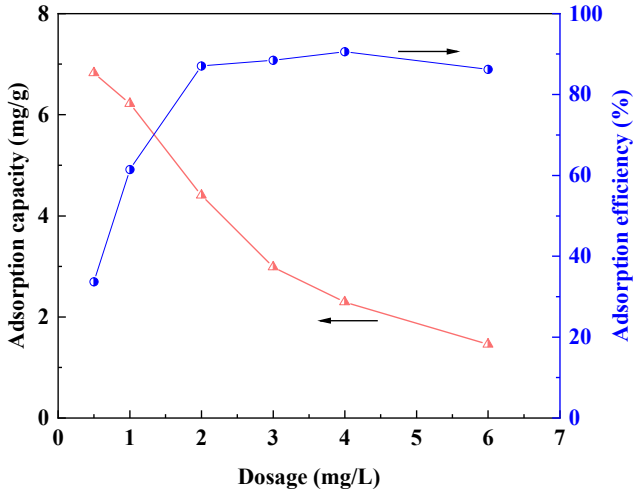


Figure 8. The effect of the NMRM dosage on removing the P from the NMRM. (10 mg/L, 25 °C, pH = 12).

The effect of the initial phosphorus concentration for removing the P of the NMRM is displayed in Figure 9. From Figure 9, with the rise of P concentration, the adsorption efficiency of NMRM to P increased initially, then reduced. However, the adsorption capacity

of the NMRM to P gradually rose to over 8 mg/g, given the rise in the initial P concentration. This is mainly because increasing the solute concentration will increase the solute diffusion rate, accelerate the adsorption to saturation, and then improve the adsorption capacity. It is also evident that, at the initial P concentration of 10 mg/L, the adsorption efficiency of the NMRM to the P was the highest, the adsorption efficiency was 71.02%, and at this time, the adsorption capacity was 3.53 mg/g.

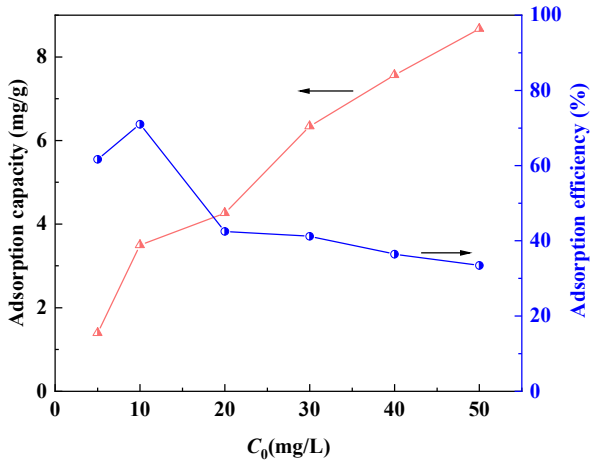


Figure 9. The effect of the P concentration on removing the P from the NMRM. (NMRM dosage = 2 mg/L, 25 °C, pH = 12).

The experimental results for the adsorption of P by the NMRM at different temperatures are displayed in Figure 10. It is obvious that the adsorption capacity and adsorption efficiency of P by NMRM showed a gradual downward trend as the temperature rose. When the adsorption temperature was increased from 25 °C to 45 °C, the adsorption capacity of P by NMRM reduced from 4.05 mg/g to 2.20 mg/g; meanwhile, the adsorption efficiency reduced from 82.80% to 44.93%. It can be concluded that the process for removing P from the NMRM was an exothermic process. Therefore, the best temperature for removing P from the NMRM in the study was 25 °C.

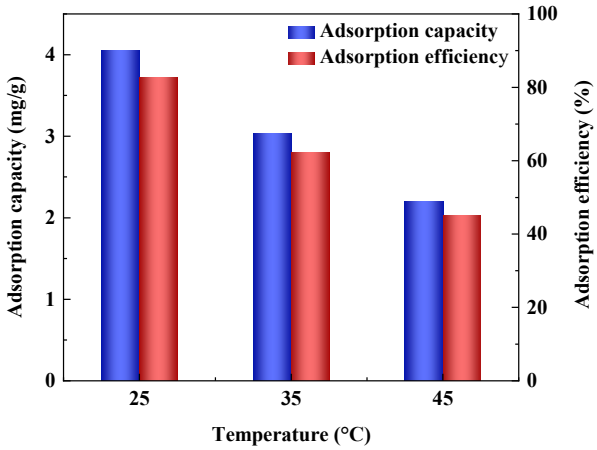


Figure 10. The effect of temperature on removing the P from the NMRM. (10 mg/L, NMRM dosage = 2 mg/L, pH = 12).

The solution pH not only affects the form of the phosphate in the solution, but also affects the surface properties of the RM. Thereby, the effect of the solution pH on removing the P from the NMRM was studied. The relevant findings are displayed in Figure 11. It is obvious from Figure 11 that when the pH changed from 2 to 6, the adsorption efficiency of P decreased from 78.89% to 72.71%. When the pH increased gradually from 4 to 12,

the P adsorption efficiency of NMRM increased gradually, and the adsorption efficiency of P rose from 72.71% to 86.34%. This could be due to the fact that, with the increase in pH values, the hydrogen phosphate in the solution dissociated gradually, and the more completely the phosphate dissociated, the more charged the ions were, and the easier it was to adsorb on the NMRM [51]. Moreover, when the pH was 12, the P adsorption efficiency and capacity of NMRM reached the maximum value, which was 86.34% and 4.19 mg/g, respectively, while under the same conditions, the adsorption effect of RM on phosphorus before modification was poor, with a P adsorption capacity of only 0.5 mg/g. The modification could significantly improve its phosphorus adsorption effect to almost eight times higher than that of the initial RM.

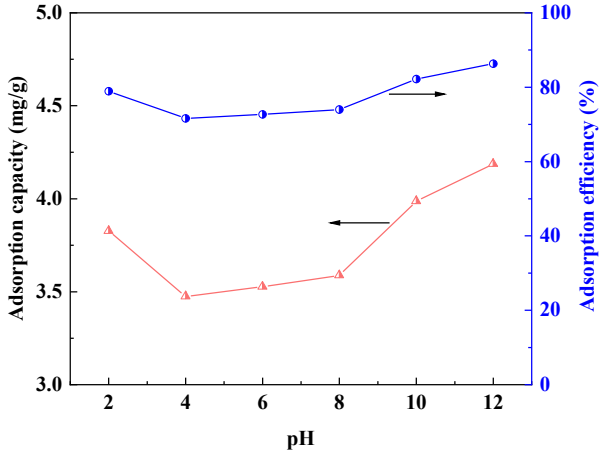


Figure 11. Effect of pH for removing P of NMRM. (10 mg/L, NMRM dosage = 2 mg/L, 25 °C).

3.3. Adsorption Kinetics

To explore the adsorption rate and kinetic mechanism involving the P adsorption on NMRM, Equations (3) and (4) were introduced in the study. Equation (3) was a model of pseudo-first-order kinetics. Equation (4) was a model of pseudo-second-order kinetics.

$$\ln(q_e - q_t) = \ln q_e - k_1 t, \tag{3}$$

$$\frac{t}{q_t} = \frac{1}{k_2 q_e^2} + \frac{t}{q_e}, \tag{4}$$

where q_t represents the t min absorption capacity (mg/g), q_e represents the equilibrium absorption capacity (mg/g), t means the absorption time (min), k_1 represents the kinetics rate constant of the pseudo-first-order, and k_2 represents the kinetics rate constant of the pseudo-second-order, respectively.

The findings from the experiment and kinetic model fitting are also displayed in Figure 12. From Figure 12a, it is clear that the P adsorption of NMRM moved along quite quickly, achieving equilibrium in about 25 min. The adsorption capacity of NMRM to phosphorus grew quickly over time, especially in the initial 5 min, and then grew slowly until reaching the adsorption equilibrium of NMRM. It could be attributed to the sufficient adsorption sites or the strong driving force generated by large concentration differences, which resulted in the quick rise of the initial adsorption capacity. When the adsorption sites of NMRM were progressively occupied by the phosphorus ions in the solution, the repulsive force generated at the interface between solid and liquid might increase, and the driving force generated by large concentration differences gradually decreased. Thus, it is clear that the adsorption rate of NMRM to phosphorus gradually decreased until it attained the adsorption equilibrium. Figure 12b,c shows the fitting curves with the kinetic models of the pseudo-first-order and the pseudo-second-order for the NMRM adsorption to phosphorus in the solutions, and the calculated parameters of the kinetic models for

the NMRM adsorption to phosphorus are also presented in Table 3. It is clear that the correlation coefficient (R^2) obtained by the pseudo-second-order model was 0.99, and was greater than that of the pseudo-first-order model, in which R^2 was 0.91. Additionally, it also can be seen that the actual experimental values (4.08 mg/g) and the predicted values of q_e acquired from the kinetic model of pseudo-second-order were almost identical. According to the above results, the kinetic adsorption of NMRM to phosphorus in the solutions was better illustrated by the pseudo-second-order kinetic equation. Meanwhile, the rate-limiting step of NMRM to phosphorus could be due to the chemical absorption between them. It could also be concluded that the existing amount of adsorption sites on the NMRM surface affected its retention rates more than the ion concentration in solutions.

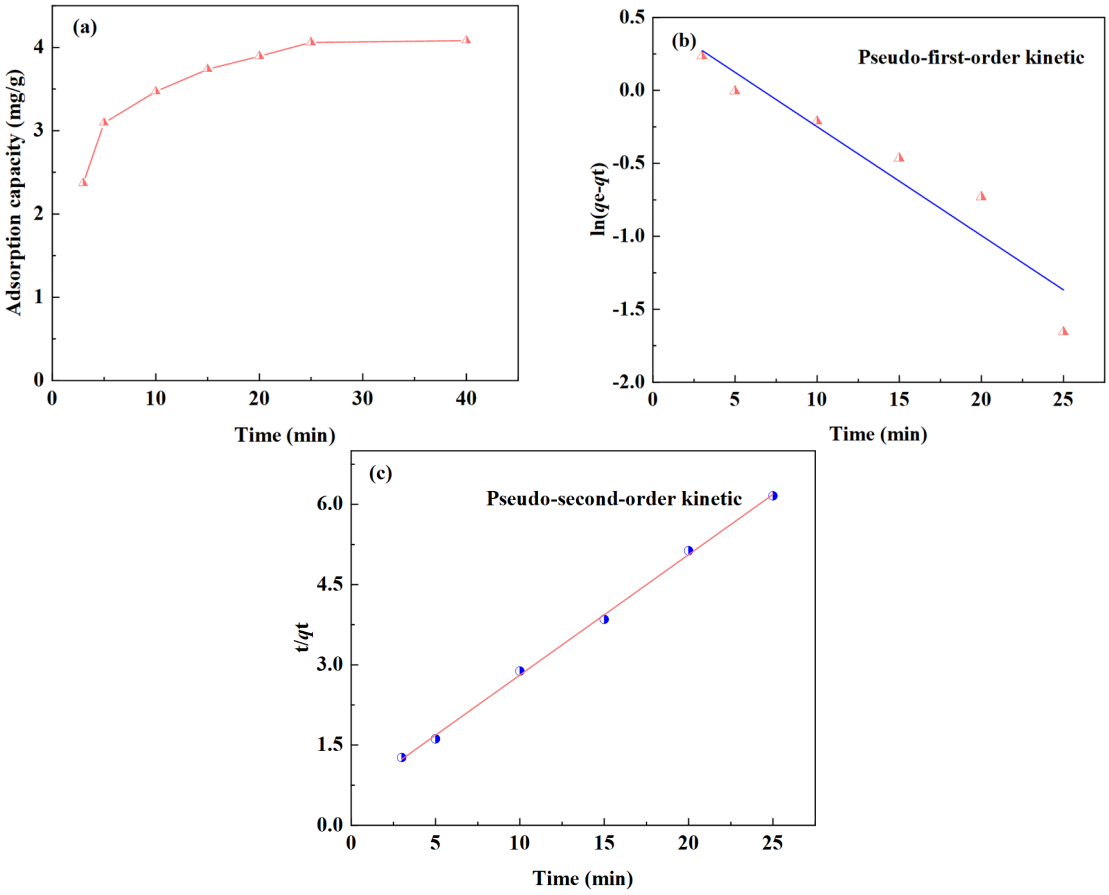


Figure 12. Effect of time on the adsorption of P by NMRM (**a**); curve fitting results of the P adsorption by NMRM with the kinetic models of pseudo-first-order (**b**) and pseudo-second-order (**c**).

Table 3. Adsorption kinetics parameters.

$q_{e,exp}$ (mg/g)	Pseudo-First-Order Kinetics			Pseudo-Second-Order Kinetics		
	k_1	q_e (mg/g)	R^2	k_2	q_e (mg/g)	R^2
4.08	0.08	3.14	0.91	0.09	4.44	0.99

3.4. Adsorption Isotherms

To evaluate the process for removing P of NMRM in the solution, the adsorption isotherm models of Langmuir and Freundlich were utilized, and could be represented by Equations (5) and (6), respectively:

$$\frac{1}{q_e} = \frac{1}{q_m K_L C_e} + \frac{1}{q_m} \quad (5)$$

$$\ln q_e = \frac{\ln C_e}{n} + \ln K_F \quad (6)$$

where q_e means the equilibrium absorption capacity (mg/g), q_m means the maximum adsorption capacity (mg/g), C_e means the P equilibrium concentration (mg/L), K_L means the Langmuir adsorption constant, and K_F and n are constants involved in adsorption capacity and intensity, respectively.

The adsorption isotherms of the P on the NMRM are displayed in Figure 13. Meanwhile, their associated computed parameters are provided in Table 4. The findings indicate that the fitted isotherm's correlation coefficient R^2 for the two models of the NMRM adsorption are 0.97 and 0.98, respectively. This indicates that the adsorption process of NMRM for phosphorus in solutions was assigned to multilayer adsorption. Meanwhile, the computed Langmuir constant K_L was 0.02 and within the range of 0 to 1, which exhibited the benefits to the adsorption process of NMRM. It could also be concluded that the adsorption process of MRM might involve some chemical and multilayer adsorption reactions, given that R^2 was not sufficiently close to 1. The saturation adsorption capacity of the NMRM to P obtained from the Langmuir isotherm model was 17.7 mg/g, which markedly contrasted with the actual value. Thus, it could be concluded that the Freundlich adsorption isotherm model could provide a more accurate description of the adsorption equilibrium of the NMRM to the P in the solution.

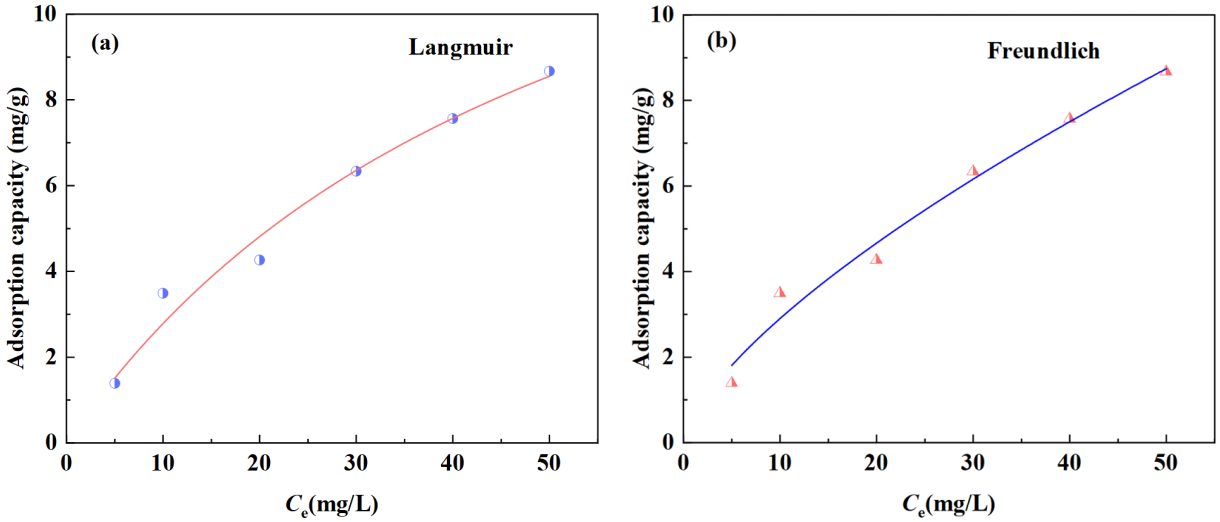


Figure 13. Adsorption isotherms of Langmuir model(**a**) and Freundlich model (**b**).

Table 4. Parameters of adsorption isotherms.

Langmuir			Freundlich		
K_L	q_m (mg/g)	R^2	K_F	n	R^2
0.02	17.7	0.97	0.60	0.69	0.98

3.5. Adsorption Thermodynamics

The adsorption thermodynamics were analyzed to measure the adsorption of NMRM for P at different temperatures. The thermodynamic parameters (ΔG^0, ΔH^0, and ΔS^0) were obtained from thermodynamic Equations (7)–(9).

$$\Delta G^0 = \Delta H^0 - T \cdot \Delta S^0 \quad (7)$$

$$\ln k_d = \frac{\Delta S^0}{R} - \frac{\Delta H^0}{R \cdot T} \quad (8)$$

$$k_d = \frac{q_e}{C_e} \quad (9)$$

where, ΔG^0 means Gibbs free energy (kJ/mol), ΔH^0 means adsorption enthalpy change (kJ/mol), ΔS^0 means entropy change (J mol^{-1} K^{-1}), T means the absolute temperature (K), R means the ideal gas constant (8.314 J/(mol·K)), and k_d means the equilibrium constant.

The linear relationship between $\ln k_d$ and $1/T$ of NMRM is depicted in Figure 14. The calculated thermodynamic parameters are given in Table 5. It is obvious from Figure 14 that the thermodynamic parameters $\ln k_d$ fitted well with $1/T$. Additionally, it is clear in Table 5 that ΔH was negative, indicating that the process of NMRM's adsorption to P was a spontaneous exothermic process, and heating up was not conducive to the adsorption of the NMRM, which indicates that NMRM had a better treatment effect on phosphorus-containing wastewater at a lower temperature. The negative ΔS from the study was due to the adsorption process of phosphorus by the NMRM in this system, accompanied by the desorption of the water molecules, and the entropy added in the desorption process of the water molecules was less than the entropy reduced in the adsorption process of phosphorus, resulting in the whole process of ΔS being less than 0. At 25 °C, ΔG was negative, indicating that the adsorption reaction between the MRM and the phosphorus was spontaneous at this temperature, and the NMRM had a strong adsorption performance for phosphorus in the solution.

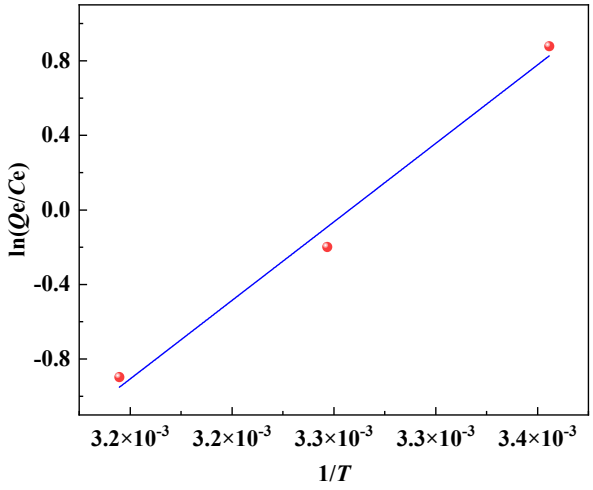


Figure 14. Adsorption thermodynamics of P on NMRM.

Table 5. Adsorption thermodynamics parameters of P on NMRM.

T (K)	ΔH^0 (kJ/mol)	ΔS^0 (J mol^{-1} K^{-1})	ΔG^0 (kJ/mol)
298			−2.05
308	−70.1	−0.23	0.24
318			2.52

3.6. Adsorption Mechanism

To study the adsorption mechanism of the novel NMRM for P, SEM and mapping EDS were conducted and analyzed, which are displayed in Figure 15. The findings reveal that, before and after P adsorption (compared with Figure 4b), the element content of P in mapping changed from 0.83% to 0.98%, which confirmed the adsorption of NMRM to phosphate in the solution.

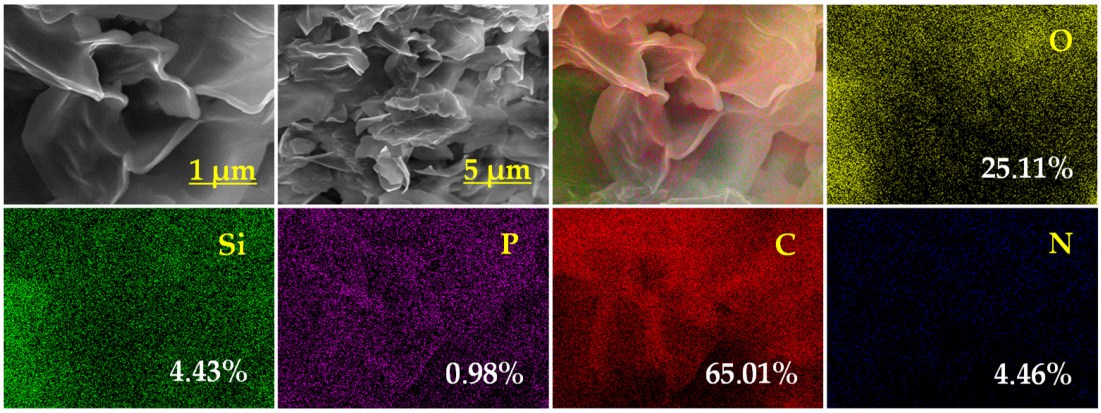


Figure 15. The SED-EDS of NMRM after adsorption.

FTIR spectra of NMRM-adsorbing P were also detected for the study of the adsorption mechanism, and the correlation analyses are displayed in Figure 16. The peak was about 2916 cm^{-1}, which appeared in the FTIR spectrum of NMRM, and could correspond to the stretching vibration of alkanes [52]. After adsorption, a new absorption peak of about 1253 cm^{-1} appeared in NMRM spectrum, corresponding to the stretching vibration of phosphate radical (PO_4^{3-}). Furthermore, the characteristic peaks of C_4N^+ in the FTIR spectrum of NMRM-adsorbing P existed remarkably as a red shift phenomenon, which moved from 1481 cm^{-1} to 1466 cm^{-1}. These findings demonstrate that there was a chemical adsorption reaction between NMRM and phosphate, which might occur at the C_4N^+ site of the NMRM.

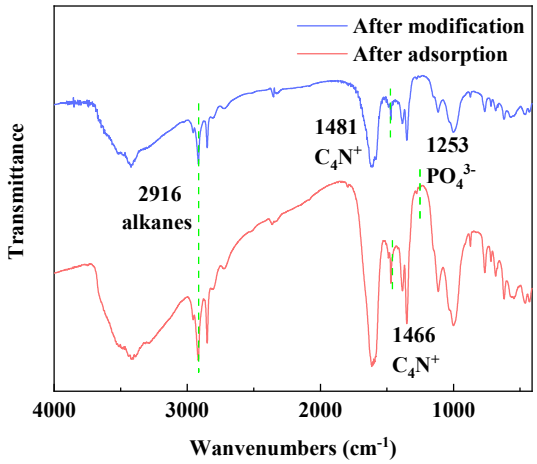


Figure 16. FT-IR of NMRM before and after adsorption.

To further explore the mechanism of phosphorus removal by the NMRM through the change in surface charge, the surface zeta potential of the NMRM before and after the phosphorus adsorption was measured in this study. The measured findings are shown in Figure 17. The zero potential point (pH_{PZC}) of the NMRM was 11.26, and its surface was positively charged in a large pH range, which was beneficial to phosphorus removal in the solution. After adsorption, the surface zeta potential of NMRM had certain changes towards the negative. The reason for this phenomenon was that there was an adsorption reaction between NMRM and phosphorus, meanwhile negative charge on the NMRM surface increased due to the adsorption of phosphorus, while they changed little. It could be concluded that the chemical adsorption reaction, which might be the ion exchange, played a significant role in removing phosphorus by NMRM in the solution [53].

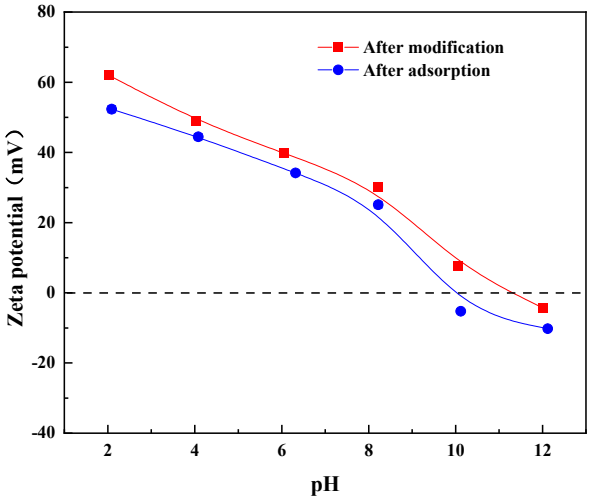


Figure 17. Zeta of NMRM before and after adsorption.

In conclusion, based on the analysis results of SEM, EDS, FT-IR, and zeta potential, the strong adsorption of the phosphorus in the solution by the NMRM could be attributed to chemisorption, mainly ion exchange.

4. Conclusions

Considering the severe environmental damage brought on by the prolonged storage of RM and phosphorus pollution, the NMRM was designed and first used to remove phosphorus from wastewater in order to achieve dual benefits for the environment. Under microwave-assisted conditions, a common third-generation environmentally friendly quaternary ammonium salt disinfectant, DDAC, was first used as the modifier to achieve one-step rapid preparation of the novel modified red-mud-based adsorption material. The analyses of the characterization results of the RM before and after modification show that the DDAC modification did not change the structure of the initial RM, but could adsorb on the surface and provide more active adsorption sites. The study of phosphorus adsorption performance indicates that the NMRM exhibited an excellent adsorption capacity to phosphorus. When the dosage of NMRM was 2 mg/L, pH was 12, and the concentration of phosphorus in solution was 10 mg/L, the adsorption efficiency was 86.34%, and the adsorption capacity was 4.19 mg/g. Under the same conditions, the phosphorus adsorption capacity of unmodified red mud was only 0.5 mg/g. The phosphorus adsorption capacity of red mud was increased by 88.07% after modification. The adsorption behavior of the NMRM matched perfectly with the Freundlich isotherm model and the pseudo-second-order kinetics model. It could be concluded that the phosphorus was chemically adsorbed on the MRM surface, which was mainly the ion exchange. RM, a widely sourced solid waste, was used to manufacture phosphorus adsorption materials with dual environmental advantages in addition to economic efficiency. Therefore, it was demonstrated that the NMRM had good prospects for the cleanup of phosphorus-containing wastewater.

Author Contributions: Conceptualization, W.L. (Wenbao Liu) and Y.S.; Data curation, W.L. (Weichao Li) and Y.Z.; Formal analysis, W.L. (Weichao Li) and S.Z.; Funding acquisition, W.L. (Wenbao Liu); Investigation, W.L. (Weichao Li) and S.Z.; Methodology, Q.Z. (Qin Zhang) and Y.S.; Software, S.Z.; Validation, W.L. (Weichao Li) and S.Z.; Visualization, W.L. (Wenbao Liu); Writing—original draft, W.L. (Wenbao Liu) and Q.Z. (Qiang Zhao); Writing—review and editing, Q.Z. (Qin Zhang) and Y.S. All authors have read and agreed to the published version of the manuscript.

Funding: This work was supported by Guizhou Provincial Science and Technology Projects (Qiankehe Support [2023] General 142), and the China Postdoctoral Science Foundation (2022M720927).

Data Availability Statement: Data are contained within the article.

Conflicts of Interest: The authors declare no conflict of interest..

References

1. Lyu, F.; Niu, S.; Wang, L.; Liu, R.; Sun, W.; He, D. Efficient removal of Pb(II) ions from aqueous solution by modified red mud. *J. Hazard. Mater.* **2021**, *406*, 124678. [CrossRef] [PubMed]
2. Lyu, F.; Hu, Y.; Wang, L.; Sun, W. Dealkalization processes of bauxite residue: A comprehensive review. *J. Hazard. Mater.* **2021**, *403*, 123671. [CrossRef] [PubMed]
3. Lyu, F.; Gao, J.; Sun, N.; Liu, R.; Sun, X.; Cao, X.; Wang, L.; Sun, W. Utilisation of propyl gallate as a novel selective collector for diaspore flotation. *Miner. Eng.* **2019**, *131*, 66–72. [CrossRef]
4. Rai, S.; Nimje, M.T.; Chaddha, M.J.; Modak, S.; Rao, K.R.; Agnihotri, A. Recovery of iron from bauxite residue using advanced separation techniques. *Miner. Eng.* **2019**, *134*, 222–231. [CrossRef]
5. Liu, W.; Chen, X.; Li, W.; Yu, Y.; Yan, K. Environmental assessment, management and utilization of red mud in China. *J. Clean. Prod.* **2014**, *84*, 606–610. [CrossRef]
6. Lyu, F.; Sun, N.; Sun, W.; Khoso, S.A.; Tang, H.-h.; Wang, L. Preliminary assessment of revegetation potential through ryegrass growing on bauxite residue. *J. Cent. South Univ.* **2019**, *26*, 404–409. [CrossRef]
7. Wang, L.; Wang, J.; Cao, Y.; Li, W.; Wang, Y.; Xu, J.; Xu, G. Molecular evidence for better efficacy of hypocrellin A and oleanolic acid combination in suppression of HCC growth. *Eur. J. Pharmacol.* **2019**, *842*, 281–290. [CrossRef]
8. Zeng, Q.; Huang, Y.; Huang, L.; Hu, L.; Sun, W.; Zhong, H.; He, Z. High adsorption capacity and super selectivity for Pb(II) by a novel adsorbent: Nano humboldtine/almandine composite prepared from natural almandine. *Chemosphere* **2020**, *253*, 126650. [CrossRef]
9. Pepper, R.A.; Couperthwaite, S.J.; Millar, G.J. Comprehensive examination of acid leaching behaviour of mineral phases from red mud: Recovery of Fe, Al, Ti, and Si. *Miner. Eng.* **2016**, *99*, 8–18. [CrossRef]
10. Zhu, F.; Li, X.; Xue, S.; Hartley, W.; Wu, C.; Han, F. Natural plant colonization improves the physical condition of bauxite residue over time. *Environ. Sci. Pollut. Res.* **2016**, *23*, 22897–22905. [CrossRef]
11. Dai, X.; Thi Hong Nhung, N.; Hamza, M.F.; Guo, Y.; Chen, L.; He, C.; Ning, S.; Wei, Y.; Dodbiba, G.; Fujita, T. Selective adsorption and recovery of scandium from red mud leachate by using phosphoric acid pre-treated pitaya peel biochar. *Sep. Purif. Technol.* **2022**, *292*, 121043. [CrossRef]
12. Bang, K.-H.; Kang, Y.-B. Recycling red mud to develop a competitive desulfurization flux for Kanbara Reactor (KR) desulfurization process. *J. Hazard. Mater.* **2022**, *440*, 129752. [CrossRef] [PubMed]
13. Habibi, H.; Mokmeli, M.; Shakibania, S.; Pirouzan, D.; Pourkarimi, Z. Separation and recovery of titanium and scandium from the red mud. *Sep. Purif. Technol.* **2023**, *317*, 123882. [CrossRef]
14. Yang, D.; Shi, M.; Zhang, J.; Sasaki, A.; Endo, M. Reductive roasting of arsenic-contaminated red mud for Fe resources recovery driven by johnbaumite-based arsenic thermostabilization strategy. *J. Hazard. Mater.* **2023**, *452*, 131255. [CrossRef]
15. Zhang, Y.; Qian, W.; Zhou, P.; Liu, Y.; Lei, X.; Li, B.; Ning, P. Research on red mud-limestone modified desulfurization mechanism and engineering application. *Sep. Purif. Technol.* **2021**, *272*, 118867. [CrossRef]
16. Mukiza, E.; Zhang, L.; Liu, X.; Zhang, N. Utilization of red mud in road base and subgrade materials: A review. *Resour. Conserv. Recycl.* **2019**, *141*, 187–199. [CrossRef]
17. Qi, L.; Sun, Z.; Tang, Q.; Wang, J.; Huang, T.; Sun, C.; Gao, F.; Tang, C.; Dong, L. Getting insight into the effect of CuO on red mud for the selective catalytic reduction of NO by NH_3. *J. Hazard. Mater.* **2020**, *396*, 122459. [CrossRef]
18. Gong, Z.; Ma, J.; Wang, D.; Niu, S.; Yan, B.; Shi, Q.; Lu, C.; Crittenden, J. Insights into modified red mud for the selective catalytic reduction of NOx: Activation mechanism of targeted leaching. *J. Hazard. Mater.* **2020**, *394*, 122536. [CrossRef]
19. Hm Ahmed, M.; Batalha, N.; Alothman, Z.A.; Yamauchi, Y.; Valentino Kaneti, Y.; Konarova, M. Transforming red mud into an efficient Acid-Base catalyst by hybridization with mesoporous ZSM-5 for Co-pyrolysis of biomass and plastics. *Chem. Eng. J.* **2022**, *430*, 132965. [CrossRef]
20. Chen, X.; Guo, Y.; Ding, S.; Zhang, H.; Xia, F.; Wang, J.; Zhou, M. Utilization of red mud in geopolymer-based pervious concrete with function of adsorption of heavy metal ions. *J. Clean. Prod.* **2019**, *207*, 789–800. [CrossRef]
21. Kaya-Özkiper, K.; Uzun, A.; Soyer-Uzun, S. Red mud- and metakaolin-based geopolymers for adsorption and photocatalytic degradation of methylene blue: Towards self-cleaning construction materials. *J. Clean. Prod.* **2021**, *288*, 125120. [CrossRef]
22. Cusack, P.B.; Healy, M.G.; Ryan, P.C.; Burke, I.T.; O'Donoghue, L.M.T.; Ujaczki, É.; Courtney, R. Enhancement of bauxite residue as a low-cost adsorbent for phosphorus in aqueous solution, using seawater and gypsum treatments. *J. Clean. Prod.* **2018**, *179*, 217–224. [CrossRef]
23. Bhatnagar, A.; Vilar, V.J.P.; Botelho, C.M.S.; Boaventura, R.A.R. A review of the use of red mud as adsorbent for the removal of toxic pollutants from water and wastewater. *Environ. Technol.* **2011**, *32*, 231–249. [CrossRef]
24. Zhu, J.; Wang, S.; Li, H.; Qian, J.; Lv, L.; Pan, B. Degradation of phosphonates in Co(II)/peroxymonosulfate process: Performance and mechanism. *Water Res.* **2021**, *202*, 117397. [CrossRef] [PubMed]
25. Wang, S.; Zhang, B.; Shan, C.; Yan, X.; Chen, H.; Pan, B. Occurrence and transformation of phosphonates in textile dyeing wastewater along full-scale combined treatment processes. *Water Res.* **2020**, *184*, 116173. [CrossRef]
26. Sun, S.; Shan, C.; Yang, Z.; Wang, S.; Pan, B. Self-Enhanced Selective Oxidation of Phosphonate into Phosphate by Cu(II)/H_2O_2: Performance, Mechanism, and Validation. *Environ. Sci. Technol.* **2022**, *56*, 634–641. [CrossRef]

27. Chen, C.; Ma, C.; Yang, X.; Demeestere, K.; Nikiforov, A.; Van Hulle, S.W.H. Phosphorus recovery from phosphonate-contaminated wastewater by nonthermal plasma treatment prior to adsorption on granular iron-coated sand. *Chem. Eng. J.* **2023**, *464*, 142753. [CrossRef]
28. Makita, Y.; Sonoda, A.; Sugiura, Y.; Ogata, A.; Suh, C.; Lee, J.-h.; Ooi, K. Phosphorus removal from model wastewater using lanthanum hydroxide microcapsules with poly(vinyl chloride) shells. *Sep. Purif. Technol.* **2020**, *241*, 116707. [CrossRef]
29. Zhang, R.; Wang, L.; Hussain Lakho, F.; Yang, X.; Depuydt, V.; Igodt, W.; Quan Le, H.; Rousseau, D.P.L.; Van Hulle, S. Iron oxide coated sand (IOS): Scale-up analysis and full-scale application for phosphorus removal from goat farm wastewater. *Sep. Purif. Technol.* **2022**, *284*, 120213. [CrossRef]
30. Wang, H.; Yu, L.-Q.; Chen, S.-N.; Liu, M.; Fan, N.-S.; Huang, B.-C.; Jin, R.-C. Coagulation enhanced high-rate contact-stabilization process for pretreatment of municipal wastewater: Simultaneous organic capture and phosphorus removal. *Sep. Purif. Technol.* **2022**, *298*, 121669. [CrossRef]
31. Ha, T.-H.; Mahasti, N.N.N.; Lu, M.-C.; Huang, Y.-H. Application of low-solubility dolomite as seed material for phosphorus recovery from synthetic wastewater using fluidized-bed crystallization (FBC) technology. *Sep. Purif. Technol.* **2022**, *303*, 122192. [CrossRef]
32. Khani, M.H.; Khamseh, A.G. Statistical analysis, equilibrium and dynamic study on the biosorption of strontium ions on Chlorella vulgaris. *J. Radioanal. Nucl. Chem.* **2023**, *332*, 3325–3334. [CrossRef]
33. Amini, Y.; Hassanvand, A.; Ghazanfari, V.; Shadman, M.M.; Heydari, M.; Alborzi, Z.S. Optimization of liquid-liquid extraction of calcium with a serpentine microfluidic device. *Int. Commun. Heat Mass Transf.* **2023**, *140*, 106551. [CrossRef]
34. Li, X.; Zhou, Y.; Ma, X.; Ding, X.; Lai, S.; Li, X.; Liu, G.; Sun, P.; Yao, H. Self-powered wastewater purification and phosphorus recovery systems with novel self-filtering Al-air batteries. *Chem. Eng. J.* **2023**, *460*, 141570. [CrossRef]
35. Rott, E.; Minke, R.; Steinmetz, H. Removal of phosphorus from phosphonate-loaded industrial wastewaters via precipitation/flocculation. *J. Water Process Eng.* **2017**, *17*, 188–196. [CrossRef]
36. Wang, R.; Zhu, W.; Zhao, S.; Cao, J. Hydrothermal oxidation-precipitation method for recovering phosphorus from dewatered sludge and the mechanisms involved. *Sep. Purif. Technol.* **2022**, *298*, 121580. [CrossRef]
37. Yu, X.; Nakamura, Y.; Otsuka, M.; Omori, D.; Haruta, S. Development of a novel phosphorus recovery system using incinerated sewage sludge ash (ISSA) and phosphorus-selective adsorbent. *Waste Manag.* **2021**, *120*, 41–49. [CrossRef]
38. Wang, B.; Ma, Y.; Lee, X.; Wu, P.; Liu, F.; Zhang, X.; Li, L.; Chen, M. Environmental-friendly coal gangue-biochar composites reclaiming phosphate from water as a slow-release fertilizer. *Sci. Total Environ.* **2021**, *758*, 143664. [CrossRef]
39. Li, S.; Huang, X.; Liu, J.; Lu, L.; Peng, K.; Bhattarai, R. PVA/PEI crosslinked electrospun nanofibers with embedded La(OH)3 nanorod for selective adsorption of high flux low concentration phosphorus. *J. Hazard. Mater.* **2020**, *384*, 121457. [CrossRef]
40. Zhao, Q.; Liu, C.; Song, H.; Liu, Y.; Wang, H.; Tian, F.; Meng, S.; Zhang, K.; Wang, N.; Mu, R.; et al. Mechanism of phosphate adsorption on superparamagnetic microparticles modified with transitional elements: Experimental observation and computational modelling. *Chemosphere* **2020**, *258*, 127327. [CrossRef]
41. Xu, R.; Lyu, T.; Zhang, M.; Cooper, M.; Pan, G. Molecular-level investigations of effective biogenic phosphorus adsorption by a lanthanum/aluminum-hydroxide composite. *Sci. Total Environ.* **2020**, *725*, 138424. [CrossRef] [PubMed]
42. Khamseh, A.G.; Ghorbanian, S.A. Experimental and modeling investigation of thorium biosorption by orange peel in a continuous fixed-bed column. *J. Radioanal. Nucl. Chem.* **2018**, *317*, 871–879. [CrossRef]
43. Li, Z.; Xiao, D.; Ge, Y.; Koehler, S. Surface-Functionalized Porous Lignin for Fast and Efficient Lead Removal from Aqueous Solution. *ACS Appl. Mater. Interfaces* **2015**, *7*, 15000–15009. [CrossRef] [PubMed]
44. Zhao, Z.; Wang, B.; Feng, Q.; Chen, M.; Zhang, X.; Zhao, R. Recovery of nitrogen and phosphorus in wastewater by red mud-modified biochar and its potential application. *Sci. Total Environ.* **2023**, *860*, 160289. [CrossRef]
45. Joseph, C.G.; Taufiq-Yap, Y.H.; Krishnan, V.; Li Puma, G. Application of modified red mud in environmentally-benign applications: A review paper. *Environ. Eng. Res.* **2020**, *25*, 795–806. [CrossRef]
46. Dai, W.; Chang, H.; Liu, J. Method for Colorimetric Determination of Phosphorus Content in Aluminum and Iron Sample, Involves Weighing Aluminum and Iron Samples in Beaker and Adding Mixed Solution of Hydrochloric acid, Nitric Acid and Perchloric Acid. CN106841063-A, 29 December 2016.
47. Nezamzadeh-Ejhieh, A.; Shirzadi, A. Enhancement of the photocatalytic activity of Ferrous Oxide by doping onto the nano-clinoptilolite particles towards photodegradation of tetracycline. *Chemosphere* **2014**, *107*, 136–144. [CrossRef]
48. Li, W.; Liu, W.; Liu, W.; Zhou, S.; Gao, S.; Shen, Y. Capture of copper cyanide complex ions based on self-assembly of ionic liquids actuation and application to cyanide wastewater. *Hydrometallurgy* **2023**, *218*, 106043. [CrossRef]
49. Zhang, W.; Deng, Q.; He, Q.; Song, J.; Zhang, S.; Wang, H.; Zhou, J.; Zhang, H. A facile synthesis of core-shell/bead-like poly (vinyl alcohol)/alginate@PAM with good adsorption capacity, high adaptability and stability towards Cu(II) removal. *Chem. Eng. J.* **2018**, *351*, 462–472. [CrossRef]
50. Peng, X.; Liu, W.; Liu, W.; Zhao, P.; Yu, X.; Wang, Y. Fabrication of eco-friendly adsorbent derived from serpentine tailings for the removal of organic dyes. *Colloids Surf. A Physicochem. Eng. Asp.* **2022**, *643*, 128761. [CrossRef]
51. Razmi, B.; Ghasemi-Fasaei, R. Investigation of Taguchi optimization, equilibrium isotherms, and kinetic modeling for phosphorus adsorption onto natural zeolite of clinoptilolite type. *Adsorpt. Sci. Technol.* **2018**, *36*, 1470–1483. [CrossRef]

52. Li, B.; Guo, J.-Z.; Liu, J.-L.; Fang, L.; Lv, J.-Q.; Lv, K. Removal of aqueous-phase lead ions by dithiocarbamate-modified hydrochar. *Sci. Total Environ.* **2020**, *714*, 136897. [CrossRef] [PubMed]
53. Chu, J.-H.; Kang, J.-K.; Park, S.-J.; Lee, C.-G. Application of the anion-exchange resin as a complementary technique to remove residual cyanide complexes in industrial plating wastewater after conventional treatment. *Environ. Sci. Pollut. Res.* **2020**, *27*, 41688–41701. [CrossRef] [PubMed]

Disclaimer/Publisher's Note: The statements, opinions and data contained in all publications are solely those of the individual author(s) and contributor(s) and not of MDPI and/or the editor(s). MDPI and/or the editor(s) disclaim responsibility for any injury to people or property resulting from any ideas, methods, instructions or products referred to in the content.